Understanding the influence of three-dimensional sidewall roughness on observed line-edge roughness in scanning electron microscopy images

Van Kessel, Luc; Huisman, Thomas; Hagen, Cornelis W.

Important note
To cite this publication, please use the final published version (if applicable).
Please check the document version above.

Understanding the influence of three-dimensional sidewall roughness on observed line-edge roughness in scanning electron microscopy images

Luc van Kessel,[a,*] Thomas Huisman,[b] and Cornelis W. Hagen[a]
[a]Delft University of Technology, Department of Imaging Physics, Delft, The Netherlands
[b]ASML Netherlands B.V., Veldhoven, The Netherlands

Abstract

Background: Line-edge roughness (LER) is often measured from top-down critical dimension scanning electron microscope (CD-SEM) images. The true three-dimensional roughness profile of the sidewall is typically ignored in such analyses.

Aim: We study the response of a CD-SEM to sidewall roughness (SWR) by simulation.

Approach: We generate random rough lines and spaces, where the SWR is modeled by a known power spectral density. We then obtain corresponding CD-SEM images using a Monte Carlo electron scattering simulator. We find the measured LER from these images and compare it to the known input roughness.

Results: For isolated lines, the SEM measures the outermost extrusion of the rough sidewall. The result is that the measured LER is up to a factor of 2 less than the true on-wafer roughness. The effect can be modeled by making a top-down projection of the rough edge. Our model for isolated lines works fairly well for a dense grating of lines and spaces as long as the trench width exceeds the line height.

Conclusions: In order to obtain and compare accurate LER values, the projection effect of SWR needs to be taken into account.

1 Introduction

As lithography techniques move toward smaller features, line-edge roughness (LER) becomes an increasingly important parameter. Consequently, accurate metrology of LER has generated much interest in recent years.[1–3]

LER is usually measured from top-down critical dimension scanning electron microscope (CD-SEM) images. As CD-SEM is a two-dimensional imaging technique, the profile along the vertical direction is not easily accessible. Most studies of LER metrology by SEM, therefore, ignore the three-dimensional (3-D) roughness profile along the sidewall's vertical direction. In this work, we will use the term LER when referring to the roughness of the measured line profile in a CD-SEM image. Sidewall roughness (SWR) will refer to the physical roughness of the on-wafer profile.

SWR can be measured by tilted or cross-section SEM or atomic force microscopy (AFM). Thick resist films exhibit near-isotropic SWR after development.[4,5] Strong anisotropy is typically observed after etch.[4,6,7] Thin resists used for recent technology nodes show strong anisotropy with striations in the vertical direction.[8,9]

The influence of SWR on CD-SEM images has been experimentally investigated by Foucher et al.[5,10] and Fouchier et al.[11,12] These experimental studies show that 3σ LER measured from CD-SEM can be significantly less—by more than a factor of 2—compared to the 3σ SWR measured by AFM. Fouchier et al.[11,12] conclude that the LER measured by CD-SEM matches the SWR measured by AFM very well if the roughest upper layers of the feature are discarded from the AFM data. However, it is likely that the SEM is most sensitive to the upper layers in which case Fig. 8 from Ref. 11 indicates the difference could be a factor of 2.

Simulation studies have also been performed.[13–15] These studies start with a known geometry and obtain corresponding CD-SEM images using full electron scattering simulations. These simulation studies all confirm that the measured 3σ LER can be up to a factor of 2 less than the true 3σ SWR. However, none of them attempt to explain where this bias comes from, or how the measured power spectral density (PSD) corresponds to the true physical PSD.

In this study, we model the most dominant effect for the bias between LER and SWR and show how the observed PSD is related to the physical PSD. We do this by simulation. We generate line-space patterns with random rough sidewalls using a model PSD. We then obtain corresponding top-down SEM images using a Monte Carlo electron scattering simulator. We find the measured LER by extracting the contours from these images, computing the measured PSD, and subtracting the white noise floor. This unbiased measured roughness can then be compared to the input roughness.

The method of generating random features, simulating an SEM image, and extracting contours is described in Sec. 2. We first show results for the simple case of no roughness in the vertical direction in Sec. 3. In Sec. 4, we move to isolated lines with 3-D roughness. Dense line-space patterns are studied in Sec. 5.

2 Method

We study a pattern of lines and spaces in resist. We start with perfectly trapezoidal lines. The sidewalls are always vertical, except in Appendix A. The sidewalls of these lines are then modulated by random roughness according to a model PSD (Sec. 2.1). To guarantee that the geometry never self-intersects, there is no roughness on top of the lines. We study the situation with roughness on top in Appendix B. The situation is sketched in Fig. 1. A more complete study should include top and bottom corner rounding and have roughness everywhere.

We then use a simulator of electron–matter interaction (Sec. 2.2) to obtain the corresponding SEM image. Contours are extracted from this image using a thresholding method (Sec. 2.3). The resulting measured power spectrum can then be compared to the known input PSD.

Our lines are 1024-nm long, with a grid spacing of $\Delta y = 1$ nm in the direction along the line. The correlation length in this direction is usually $\xi = 10$ nm unless mentioned otherwise. The choice of Δy coincides with the pixel size of the SEM images, which is 1 nm in both x and y directions. This was done to avoid any aliasing effects. In the vertical direction, where we sometimes choose a smaller correlation length, we used a grid spacing of $\Delta z = 0.5$ nm.

The resist lines are made of PMMA, the substrate is silicon. Assuming identical roughness parameters, we have performed the same study with silicon lines on a silicon substrate. The results were very similar. This gives confidence that the results are general: they are dominated
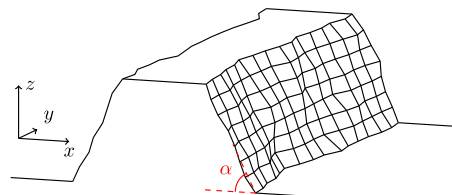
Fig. 1 Sketch of the line profile studied in this work. We start with a trapezoidal structure. The sidewalls are randomly displaced by a roughness model, while the top and substrate remain flat. Also shown is our choice of coordinate system and definition of sidewall angle α. In the main text, we only consider lines with $\alpha = 90$ deg. Different sidewall angles are used in Appendix A.

by the geometry of the sample and not material contrast. In reality, the roughness of resist (after development) and silicon (after etch) features are very different, but it appears that the SEM response to roughness is not very material dependent.

2.1 *Generation of Rough Features*

We use the method of Thorsos[16] to generate rough sidewalls. As explained by Mack,[17] the variance of the data produced by this method is biased compared to the intended value. Additionally, because the roughness is periodic, the shape of the PSD is biased if the length of the feature is on the order of the correlation length.

The bias is small when $\Delta x \ll \xi \ll L$, where Δx is the grid spacing, ξ is the correlation length of the roughness spectrum, and L is the total size of the domain. In the direction along the line, this requirement is automatically satisfied by our choices of Δx, ξ, and L. In the vertical direction, however, it is often the case that ξ is close to L or larger. Our solution is to use the Thorsos method to generate much higher sidewalls than required and use only a section of the desired size. After this step, the generated PSD closely follows the intended profile. Any remaining bias between the target and true 3σ SWR is small, but we subtract the mean and scale the amplitudes to guarantee that the 3σ SWR is exactly as intended.

We use the following model PSD:

$$\text{PSD}(f_y, f_z) = \frac{4\pi H \xi_y \xi_z \sigma^2}{[1 + (2\pi f_y \xi_y)^2 + (2\pi f_z \xi_z)^2]^{H+1}}. \tag{1}$$

This is the PSD suggested by Palasantzas,[18] modified to allow for different correlation lengths ξ_y and ξ_z in the y and z directions, respectively. H is the Hurst exponent, which is the same in all directions, and σ is the root-mean-square roughness. f is the spatial frequency, 1/wavelength. See Appendix C for details on how this PSD follows from Palasantzas's original isotropic form.

The one-dimensional version of this PSD is given by

$$\text{PSD}(f) = \frac{\Gamma\left(H + \frac{1}{2}\right)}{\Gamma(H)} \frac{2\sqrt{\pi}\xi\sigma^2}{[1 + (2\pi f\xi)^2]^{H+1/2}}, \tag{2}$$

where $\Gamma(x)$ is the gamma function.

2.2 *SEM Simulator*

SEM images are simulated using a Monte Carlo electron tracing method. Electrons can undergo three types of scattering: elastic in which electrons are deflected but keep their energy; inelastic in which electrons lose energy and may create a secondary electron; and boundary crossing.

Elastic scattering is described by Mott scattering, calculated by solving the Dirac equation in a model potential around an atom. We use the ELSEPA program[19] to compute these cross sections. At low energies (<100 eV), we transition to electron–acoustic phonon scattering, as described by Schreiber and Fitting.[20]

Inelastic scattering is described by a dielectric function model. We use measured optical data,[21] extended to nonzero momentum by the full Penn algorithm.[22] Our numerical implementation follows the description of Shinotsuka et al.[23]

Finally, near a material interface, an electron may be either reflected or transmitted and refracted due to the difference in inner potential. We use a simple quantum mechanical step function model to determine these coefficients.

Our simulator runs on graphics cards using the method of Verduin et al.[24] to allow a large-scale simulation study. A typical simulation run, with more than 10 million triangles making up the rough line geometry and more than 200 million primary electrons at 300-eV landing energy, takes <10 min on an Nvidia GTX1080.

2.3 *Contouring Method*

A large variety of contouring methods is available in the literature. The reason why this large variety exists is that a simple thresholding method is plagued by robustness issues due to SEM noise. Filtering solves the robustness issue, but filters along the direction of the line must be avoided because they inevitably also affect the LER signal.

Alternative methods based on fitting reference linescan models[25,26] do not rely on filtering or a threshold and work well even for very noisy images. However, such methods assume that the linescan—and with it, the sidewall's vertical profile—is the same for every position along the line. The applicability of these methods has not yet been proven for features with SWR, and therefore, we do not use such a method.

We opted for a simple thresholding method with minimal filtering to make it robust. We have set the threshold to 60% between the minimum and maximal signal of every linescan. This value does not significantly influence our results unless the feature has a sidewall angle or the trenches are narrower than the height of the lines. These situations are further discussed in Appendix A. We use a $\sigma = 1$ nm Gaussian blur in the direction perpendicular to the line. Since this filter does not operate in the direction along the line, it does not affect the measured PSD as strongly as a parallel filter. Using simulated images with very low noise as a benchmark, we have empirically determined that a $\sigma = 1$ nm Gaussian blur does not noticeably affect the measured PSD.

Despite this, the SEM signal in a linescan may cross the threshold multiple times. Only when the slope is as expected (i.e., positive for a left edge, negative for a right edge) do we consider a threshold crossing as a candidate for edge detection. In the exceedingly rare case that there are still multiple candidates, we select the one closest to the mean edge position.

Because this is a simulation study, we can make the noise levels in the SEM images arbitrarily low. We have used 100 electrons per pixel, disabled Poisson shot noise from the electron source, and excluded detector noise. This gives images that are less noisy than those from a real CD-SEM. Due to higher noise in real SEM images, and due to effects such as shrinking and charging, a more sophisticated contouring algorithm may be required for real SEM images.

We now have a set of measured edge positions, one for each edge in the image. The PSDs for each of these edges can be determined and averaged. Though the contouring method always finds a reasonable edge position, it remains sensitive to statistical noise of the SEM. Assuming that the noise is uncorrelated from pixel to pixel, this manifests itself as a white "noise floor," which can be subtracted from the measured PSD.[3,27]

If the noise floor is very low, the measured PSD is not always completely flat at high frequencies. We measure the height of the floor by fitting the function

$$\text{PSD}(f) = af^{-b}e^{-cf^2} + d \tag{3}$$

on a log scale to the highest half of the frequencies. The f^{-b} term represents the typical power-law behavior at high frequencies. The e^{-cf^2} term accounts for possible additional quenching of high frequencies due to the finite width of the electron beam. d is the actual noise floor.

Though Eq. (3) makes many assumptions about the shape of the PSD at high frequencies, we only use this procedure to measure d. The value of d is not very sensitive to the exact form of the fit function, but we chose Eq. (3) because it can be physically justified.

3 No Vertical Roughness

We first study the case without vertical roughness. We use the PSD of Eq. (2) with $\sigma = 1$ nm, $\xi = 10$ nm, and $H = 0.5$. We study dense lines and spaces with a 32-nm half pitch.

The measured PSD, for an infinitely narrow electron beam with 300-eV landing energy, is shown in Fig. 2(a). It also shows the measurement of the noise floor using the fit of Eq. (3). Figure 2(b) shows the same PSD with the noise floor subtracted. The measured PSD differs from the input PSD only in the very high frequencies. This divergence is most likely due to uncertainty in the noise floor measurement due to our choice of fitting function. We have run the same simulation with different electron beam landing energies (300, 800, and 3000 eV) and with a smaller x-pixel size (0.5 nm). The results were practically indistinguishable from
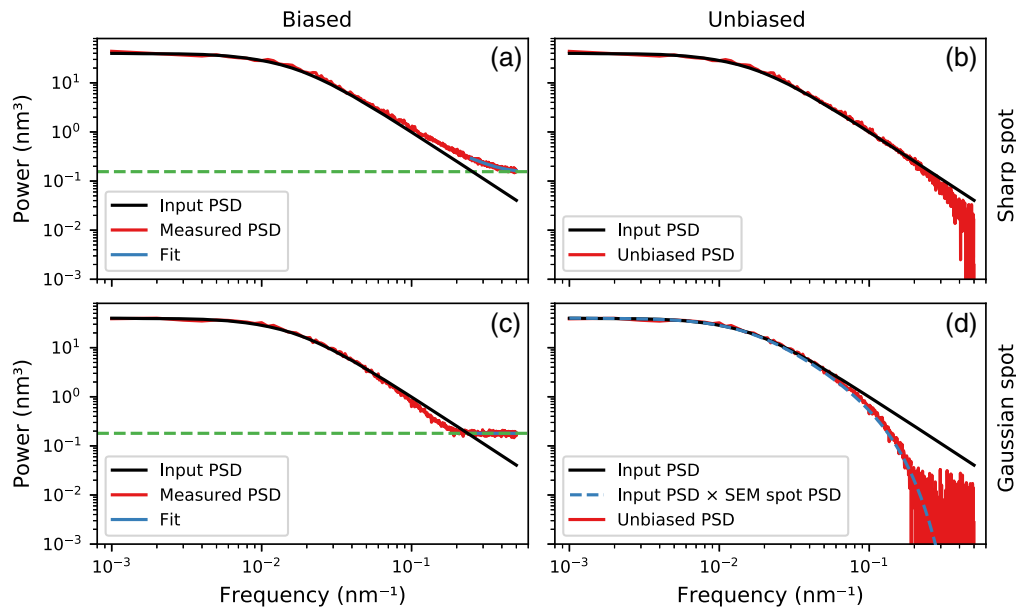
Fig. 2 The input PSD (black curve) is compared to the PSD measured from simulated SEM images (red curves). There is no roughness in the vertical direction. (a), (c) The measurement of the noise floor and (b), (d) the result after noise floor subtraction. In (a) and (b), the electron beam is infinitely sharp; in (c) and (d), the electron beam has a Gaussian profile with 3-nm FW50. The dashed curve in (d) indicates the input PSD convolved with the SEM spot.

Fig. 2(b). This implies that the high-frequency divergence in Fig. 2(b) is not due to the electron scattering cascade or material parameters.

In Figs. 2(c) and 2(d), we use a more realistic Gaussian profile for the electron beam. The full width containing 50% of the current (FW50) is 3 nm, similar to current CD-SEMs. The effect of this finite spot size is a suppression of the PSD at higher frequencies. This can be modeled by convolving the PSD of the line by the PSD of the spot. The blurring effect due to the finite spot size is a very dominant effect.

Because the effect of a finite electron beam spot size can be modeled well with a convolution, all future simulations in this work will be performed with an infinitely sharp beam.

4 Isolated Lines

We now also add roughness in the vertical direction according to Eq. (1). For simplicity, we consider isolated lines first before going to dense lines and spaces in the next section. The energy of the electron beam remains 300 eV. The effect of larger beam energies is investigated in Appendix D.

We will use the following simplistic model to understand the results. A typical SEM signal is bright when the beam lands near a sharp edge, because electrons may escape from the side. We may expect that when the beam lands on an extrusion on the rough sidewall, the SEM signal is also very bright. This means the SEM contour will go around all extrusions as seen from the top. We call this the "projection model," which is illustrated in Fig. 3.

Numerically, the projection model can be quantified by generating a random 3-D rough sidewall. Then at each position along the line, the maximum excursion in the vertical direction is taken. In this paper, we repeat this procedure for a very large number of sidewalls and find the average PSD. We have not been able to find an analytical expression.

The projection model gives a vertical averaging effect. If the correlation length in the vertical direction ξ_z is very large, the structure looks as though there is no roughness in the vertical direction. Hence, the measured PSD will be similar to the PSD of a single slice of the structure. If ξ_z is very small, the projection model averages over many correlation lengths in the vertical direction. Hence, the observed mean edge position will shift outward, and the roughness will be
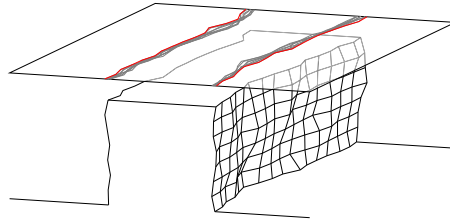
Fig. 3 Illustration of the projection model. An example 3-D rough line is shown. The contour of every slice of the geometry is projected onto the plane above the feature (gray lines). The red lines follow the outermost extrusions of the gray lines. The projection model assumes that the SEM observes this red line.

less than that of a single slice. The amount of averaging depends on the number of correlation lengths in the vertical direction: scaling both the height of the feature and ξ_z by the same factor gives the same final result.

A typical SEM image of an isolated 3-D rough line is shown in Fig. 4(a). This figure also shows the contours detected by the contouring algorithm, the true contour of the top slice of the line, and the projection model's contour. By eye, it is already clear that the projection model predicts the SEM contour quite well. Figure 4(b) shows a selected scanline from Fig. 4(a). This confirms the effects that lead us to hypothesize the projection model. The SEM signal already brightens for $x < 16$ nm (where the top of the line is), which is a well-known effect. The signal remains bright in the range 16 nm $< x <$ 19 nm, where the electron beam lands on the various extrusions of the sidewall. The edge detected by the contouring algorithm is, therefore, close to the outermost extrusion.

The accuracy of the projection model can be verified by comparing its predicted PSD to the measurement by the SEM. Such a comparison is shown in Fig. 5. The agreement between the projection model and the SEM measurement is excellent. The SEM measurement slightly under-estimates the signal at very high frequencies, similar to the situation of Fig. 2.

It is clear from Fig. 5 that the measured 3σ LER (given by the area below the blue curve) is significantly biased compared to the true 3σ SWR (given by the area below the black curve). This is consistent with the simulation and experimental studies mentioned in the introduction.[5,10–15]

Figure 6 shows the bias of measured 3σ values for a range of ξ_z/h, where h is the height of the feature. We have included the effect of the CD-SEM's spot size in this figure. The full SEM simulations were done with a Gaussian electron beam spot. The projection model was convolved with the appropriate spot PSD (as in Fig. 2). The agreement between the projection model and the full simulations is quite satisfactory.

Interpreted differently, Fig. 6 predicts that measured LER scales with film thickness if the on-wafer SWR is constant. This is a pure metrology effect. It is consistent with previous
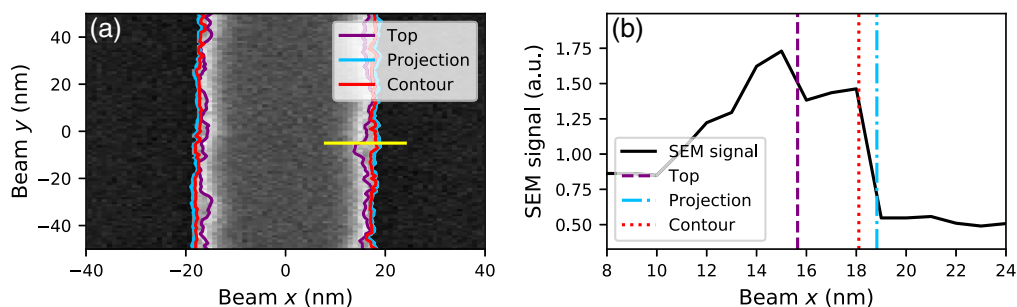
Fig. 4 (a) Typical SEM image of an isolated 3-D rough line. The contour detected by the contouring algorithm (red curve) as well as the contour of the top slice (purple) and the projection model (blue) are overlaid. The yellow horizontal line marks a selected scanline, which is reproduced in (b). The black curve represents the grayscale value of the SEM image. The positions of the top, projection model, and SEM contour are shown as vertical lines. This is an 80-nm high line with $\sigma = 1$ nm, $\xi_y = \xi_z = 10$ nm, and $H = 0.5$.
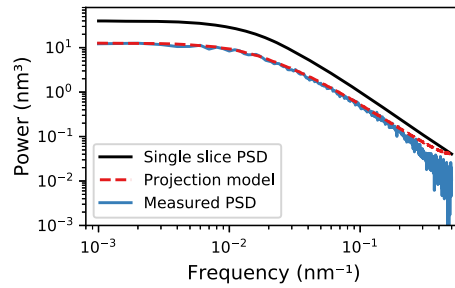
Fig. 5 The input PSD of a single slice in the sidewall (black curve) is compared to the PSD predicted by the projection model (red) and the PSD measured by SEM (blue). This figure was made for the same parameters as Fig. 4.
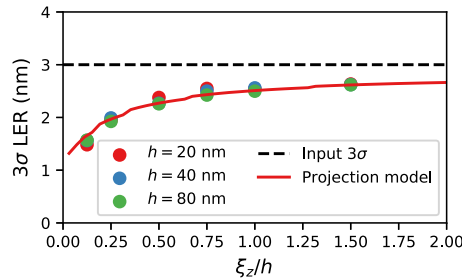
Fig. 6 Comparing the bias in 3σ LER predicted by the projection model (solid curve) to observations from SEM images for a range of heights (points). The dashed black line indicates the true 3σ SWR. This figure was made for $\xi_y = 10$ nm and $H = 0.5$. A 3-nm FW50 Gaussian spot for the CD-SEM is included in these simulations.

experimental observations,[28,29] where LER is seen to increase as resist thicknesses are reduced. It is possible that a similar metrology component plays a role in those experimental studies in addition to any change in on-wafer roughness.

As shown by Verduin et al.,[15] the correlation length measured by CD-SEM is biased if there is roughness in the vertical direction. We quantify this effect in Fig. 7(a). According to the projection model, only the ratio $\xi_{measured}/\xi_y$ is biased: scaling ξ_y results in a scaling of the PSD to lower or higher frequencies, while the shape is preserved. The bias in measured correlation length shows an interesting trend. If there are many correlation lengths in the vertical direction (small ξ_z/h), the measured correlation length is significantly smaller than the true correlation
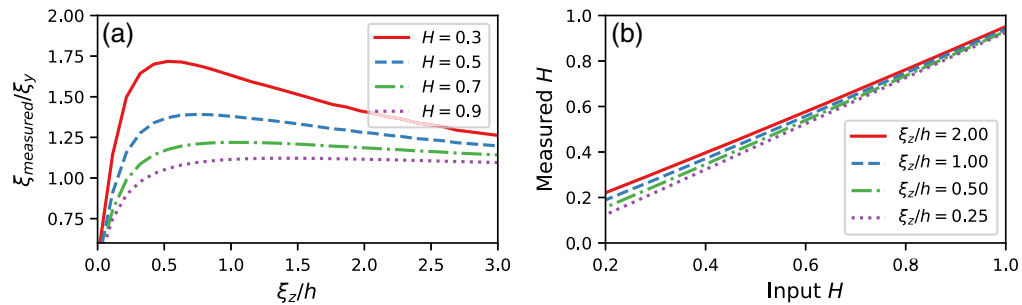
Fig. 7 The bias in the measured correlation length and Hurst exponent predicted by the projection model. The horizontal axis in figure (a) indicates the number of correlation lengths in the vertical direction; the vertical axis shows the measured correlation length relative to the true correlation length along the line. The horizontal axis in figure (b) indicates the true Hurst exponent; the vertical axis shows the measured Hurst exponent. The lines are predictions from the projection model and full SEM simulations are not shown.

length in the horizontal direction. When the structure is approximately two correlation lengths high, the measured correlation length peaks at a larger value than the true correlation length in the horizontal direction. For large ξ_z/h, the situation becomes similar to the case when there is no vertical roughness and the bias disappears.

It can be seen in Fig. 5 that the projection model gives a lower Hurst exponent than the input PSD. We quantify this bias in Fig. 7(b). The bias is almost linear, but it depends on ξ_z/h. As ξ_z/h approaches infinity, the absence of vertical roughness should make the measured H equal to the input value. The curves in Fig. 7(b) seem to agree with that trend.

We conclude this section by restating that the projection model predicts the SEM contour and its PSD very well for isolated lines. The projection model follows from purely geometrical arguments. This makes it very simple to understand and quantify. We did not attempt to find an analytical expression for the projection model PSD, but it is computationally very cheap to find numerical approximations by brute-force Monte Carlo simulation. This enables building a large library to translate "projected PSDs" back to the true sidewall PSD.

5 Dense Lines and Spaces

We are now interested in the more common situation of a dense pattern with 50% lines and 50% spaces. An example SEM image is shown in Fig. 8.

Comparing Fig. 8 to Fig. 4, we observe that some parts of the sidewall are darker in the dense line-space pattern. It is likely that electrons escaping from lower layers of the structure are blocked by the neighboring walls. As a result, those deeper layers show up darker in the SEM image. Parts of the image that are darker than the SEM contouring threshold are not considered part of the line. Therefore, the projection model does not predict the SEM contour as well as it did for the case of purely isolated lines.

We will now attempt to model this effect. Because the SEM image gets progressively darker for deeper layers, we may hypothesize that the contouring threshold for the SEM image translates to a threshold depth in the actual resist pattern. We may expect that all sidewall features above this depth become part of the SEM contour. All sidewall extrusions below this depth are too dark, and the contouring algorithm considers them part of the trench. Therefore, we will investigate a "cut-off projection model," in which we assume that the SEM contour follows the projection model above a certain cut-off depth, which we need to calibrate. A typical result is shown in Fig. 9. This result was obtained by tuning the projection model's cut-off depth such that its low-frequency PSD(0) matches the measured PSD(0).

The match between model and measured PSDs in Fig. 9(b) is much worse than in Figs. 2 and 5. High frequencies are much more suppressed in the SEM image than the simple cut-off projection model predicts. The same is also clear from the real space Fig. 9(a), where the cut-off projection model does not follow the SEM contour very closely despite our efforts to match the PSDs. This indicates that the cut-off projection model is too simplistic. This is unfortunate, but not very surprising. There are other effects at play in the image formation of an SEM. Sharp
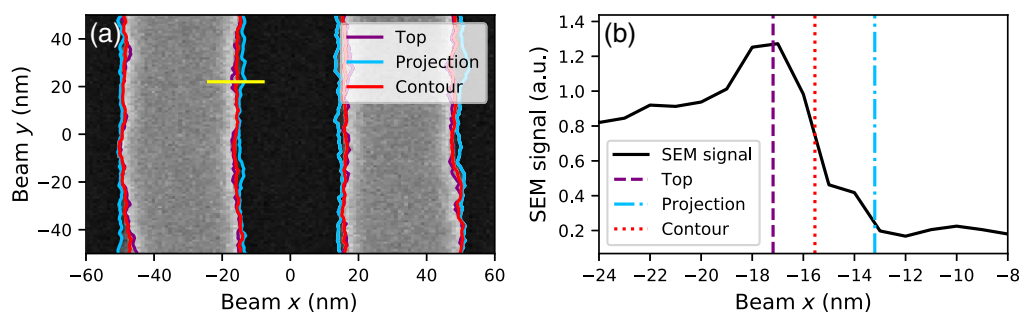
Fig. 8 Same as Fig. 4, with trenches between the lines. (a) An SEM image with the true positions of the top slice and projection model overlaid as well as the contour detected using the image. (b) A selected line of the image, marked by the horizontal yellow line in (a). The resist lines are 80-nm high, trenches are 32-nm wide.
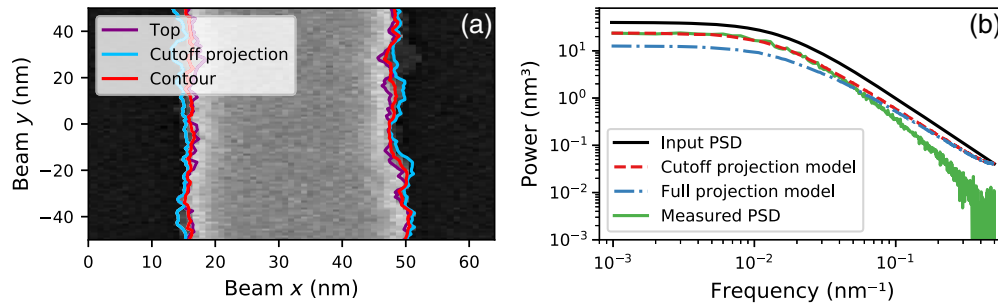
Fig. 9 (a) Same as Fig. 8, but the light blue curve now shows the projection model with a cut off at 30-nm depth. (b) Corresponding PSDs. The 30-nm cut-off depth was chosen to match the measured PSD(0).
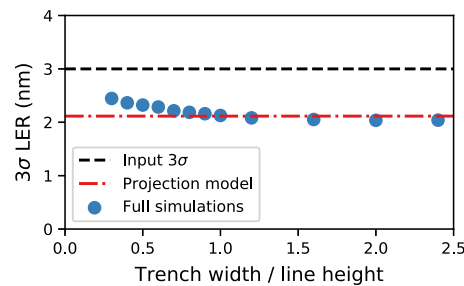
Fig. 10 The bias in measured 3σ LER as a function of trench width. These simulations were done for 40-nm high lines, with $\xi_y = \xi_z = 10$ nm and $H = 0.5$.

geometric contrast generally makes the image bright, which is why the projection model works well. But the extrusions on the sidewall, which are of the order $\sigma = 1$ nm large in one direction, are smaller than the interaction volume of the incoming electrons. Therefore, it is likely that the exact brightness in the image depends on the local geometry of the sidewall and not just the depth. Some features above our chosen cut-off depth may, therefore, be darker than the contouring threshold, whereas some features below the cut-off depth may be brighter. The relation between the measured PSD and the contouring threshold is discussed in Appendix A.

We now ask under what conditions lines can be considered "isolated enough" for the projection model (without cutoff) to be applicable. Figure 10 shows how the measured 3σ values evolve as trenches become wider. When the trench is wider than the feature height, the projection model predicts the measured 3σ value quite well. The projection model becomes worse as the trenches get narrower than the line height.

6 Conclusion

We have studied the influence of SWR on LER measured by top-down CD-SEM. This was done by generating features with known SWR, simulating corresponding CD-SEM images, and measuring LER from those images.

We have verified that the popular method of PSD analysis works very well if the structures have no roughness in the vertical direction. The dominant factor limiting the measurement of the true on-wafer PSD is the electron beam's spot size. This causes a blurring effect, suppressing the PSD at high spatial frequencies.

If the structures are isolated and rough in the vertical direction, the CD-SEM observes the outermost extrusion over the full height of the structure. This is the case for PMMA lines on a silicon substrate as shown here, but we have also verified this for silicon lines on a silicon substrate. This simple geometrical interpretation is, therefore, not due to material contrast and it is not sensitive to details of the electron scattering process. It is, therefore, likely that this effect

exists for arbitrary feature shapes. We have verified this explicitly for trapezoids with a sidewall angle (see Appendix A) and lines with roughness on the top (Appendix B).

As a result of this projection effect, the PSD measured by the SEM is biased significantly. In particular, the 3σ LER, which is often considered the most important quantity, suffers heavily from this bias.

For dense lines and spaces, the situation is complicated by the fact that the SEM is less sensitive to the lower layers. As a result, the measured PSD lies between the PSD of the top slice and that of the projection model. Empirically, we have found that the projection model works well as long as the trenches between the lines are wider than the line height.

The ultimate goal of roughness metrology is usually to predict device performance or statistical defects, not to measure the true SWR of resist patterns. An interesting question is whether subsequent process steps (such as etch) undergo a similar projection effect as top-down CD-SEM measurements. If that turns out to be the case, an LER measurement by CD-SEM may be a good predictor of device performance. However, this work shows that care must be taken for dense line-space patterns (and most likely contact holes), because the SEM is most sensitive to upper layers, which is unlikely to be the case for etch. Also, if CD-SEM is used for benchmarking and improving resists, the full SWR is an interesting quantity. We have shown that measured LER depends on film thickness, highlighting the importance of benchmarking resists under identical circumstances.

7 Appendix A: Contouring Threshold

Throughout this paper, we have used a contouring threshold of 60% between the minimum and maximum of the SEM signal. This is a common choice in industry. Most of our results are not sensitive to the choice of contouring threshold, with two situations.

7.1 *Sidewall Angle*

When there is a sidewall angle, the projection model works well for isolated lines. One thing to note is that the contouring threshold should not be set too high.

Figure 11(a) shows an SEM linescan over a trapezoidal edge without any roughness. Figure 11(b) shows an SEM image of a line with a rough sidewall (as illustrated in Fig. 1). Setting the contouring threshold too high puts the contour on top of the sidewall rather than near the outermost edge. This also makes it very sensitive to noise. High contouring thresholds should, therefore, be avoided: not because the projection model fails, but also because the contouring algorithm becomes too sensitive to noise.

After doing many simulations, we conclude that the projection model works well when the contouring threshold is 60% or less. Higher thresholds than 60% are very uncommon in the literature. For practical purposes, we conclude that the projection model works not just for vertical sidewalls, but also when the line has a sidewall angle.
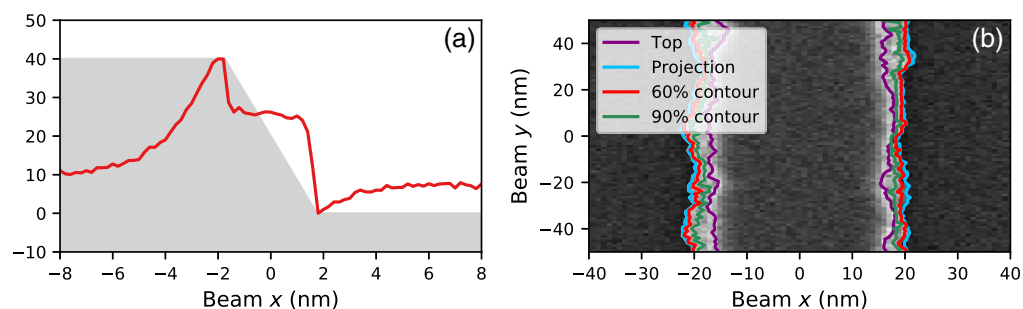
Fig. 11 SEM images of isolated trapezoidal structures, 40-nm high and with an 85-deg sidewall angle. (a) SEM linescan over a structure without any roughness. The shaded area represents the shape of the structure. (b) SEM image of an isolated 3-D rough line. The red and green curves show the measured contour lines at different threshold settings. The roughness parameters are the same as in Fig. 4.
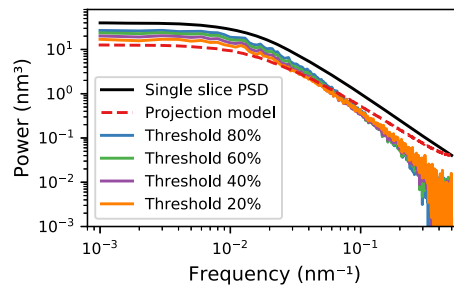
Fig. 12 Measured PSDs for various contouring thresholds in dense lines and spaces. Physical parameters are the same as in Fig. 9.

7.2 *Dense Lines and Spaces*

As discussed, lower layers of dense lines and spaces are darker in SEM images due to a shadowing effect from neighboring lines. This effect can be seen in Fig. 8. By eye, it is clear that a lower contouring threshold will put the SEM contour closer to the projection model. An obvious question now is whether the projection model becomes more applicable as the contouring threshold is lowered, and, if so, whether it is possible to find a threshold setting for which the projection model can be universally trusted.

Typical PSDs are shown in Fig. 12 for various contouring thresholds. As the contouring threshold is lowered, the measured PSD becomes more similar to the projection model: the PSD at low frequencies decreases while the PSD at high frequencies increases. However, even at a very low 20% contouring threshold, the difference remains obvious. It is conceivable that an even lower contouring threshold will eventually match the projection model, but judging from the trend in Fig. 12, this looks unlikely. Even if there is a very low threshold for which the projection model is matched, this will not be a practically useful threshold because such extreme contouring thresholds are very sensitive to SEM noise. Therefore, we conclude that there is no practical threshold setting in which the projection model becomes applicable for these very dense lines and spaces.

8 Appendix B: Top Roughness

Resist features have roughness everywhere not only along the sidewall. The projection model predicts that roughness on the top of the resist does not influence the measured LER. It is good to verify this.

We study resist lines with roughness only on the top, as illustrated in Fig. 13. The sidewalls are now flat, and the sidewall angle is 90 deg. If the projection model is correct, the SEM contour is pure white noise. The roughness on top of the feature is described by the same PSD as before, Eq. (1), with $\sigma = 1$ nm, $\xi_x = \xi_y = 10$ nm, and $H = 0.5$.

Simulation results are shown in Fig. 14. Figures 14(a) and 14(c) show contoured SEM images. Figures 14(b) and 14(d) show the measured PSDs. The noise floor was not subtracted from the measured PSDs. The measured PSDs are almost flat but not perfectly.

We have the following explanation for this effect. The top roughness is clearly visible in the SEM images. Because of this, the brightness of the line edges is also modulated. The brightness
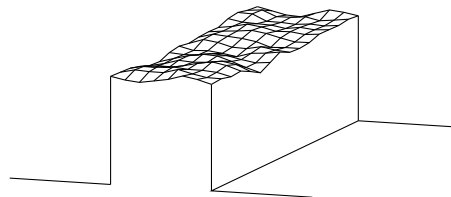
Fig. 13 Sketch of the line profile studied in Appendix B. We study lines with perfectly straight and vertical sidewalls. The top of the resist is modulated by a roughness model.
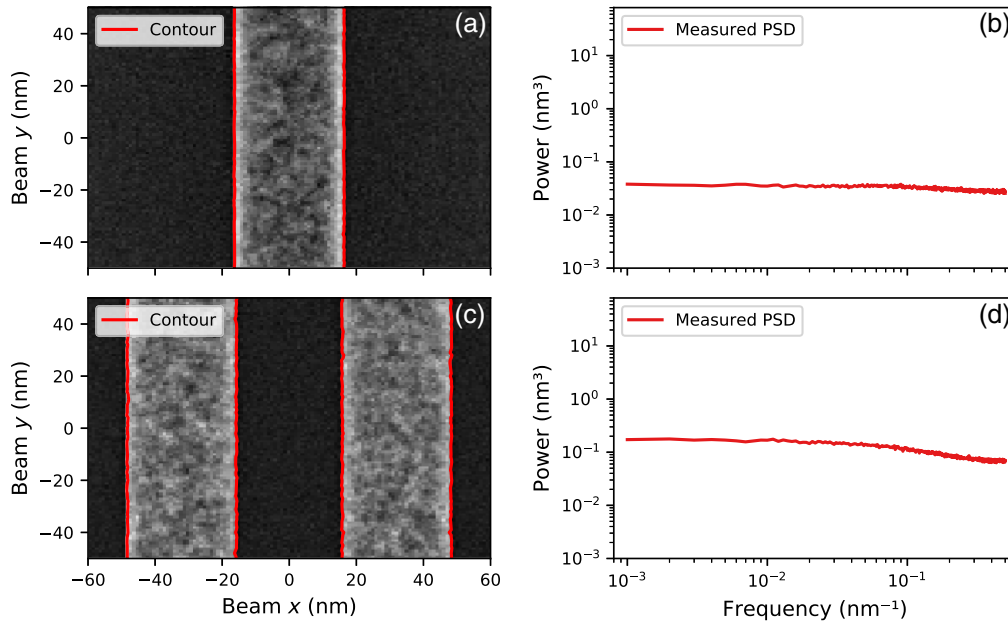
Fig. 14 Simulated SEM images and measured PSDs for features with roughness on top of the lines only, as illustrated in Fig. 13. (a), (b) For isolated lines and (c), (d) for dense lines and spaces. The noise floor was not subtracted from the measured PSDs in (b) and (d).

of the substrate is (on average) constant. The bright parts of the edge push the measured contour slightly outward, hence the top roughness "leaks" into the measured LER. However, this effect is negligible compared to the usual power contained in LER signals (cf., Figs. 2, 5, and 9). We estimate that the total variance due to nonwhite noise in Fig. 14(b) is 0.0014 nm^2. In Fig. 14(d), this is 0.011 nm^2.

9 Appendix C: Mathematical Details of the PSD

Roughness is often characterized in terms of the autocovariance function $R(x)$. A common choice is a stretched exponential[30]

$$R(x) = \sigma^2 \, \exp\left(-\left|\frac{x}{\xi}\right|^{2\alpha}\right),\tag{4}$$

where α is the roughness exponent.

In this work, we have used the PSD of Palasantzas,[18] which corresponds to the following autocovariance function:

$$R(x) = \frac{2^{1-H}\sigma^2}{\Gamma(H)}\left|\frac{x}{\xi}\right|^H K_H\left(\left|\frac{x}{\xi}\right|\right).\tag{5}$$

$K_H(x)$ is the modified Bessel function of the second kind. If $H = 1/2$, this is identical to the autocovariance of Eq. (4) with $\alpha = 1/2$. For $H \neq 1/2$, Eqs. (4) and (5) remain similar, with H taking the role of α. The main advantage of Palasantzas's choice is that the PSD has a known analytical form for all roughness exponents.

The 1-D-PSD, Eq. (2), can be obtained by Fourier transformation of Eq. (5)

$$\text{PSD}(f) = \int_{-\infty}^{\infty} \mathrm{d}x \, e^{-2\pi i f x} \frac{2^{1-H}\sigma^2}{\Gamma(H)}\left|\frac{x}{\xi}\right|^H K_H\left(\left|\frac{x}{\xi}\right|\right),\tag{6}$$
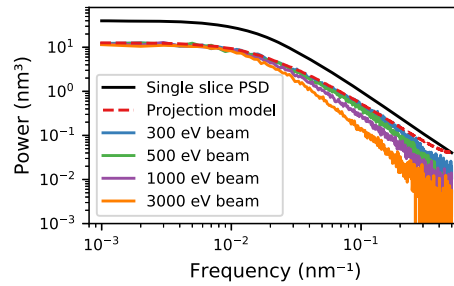
Fig. 15 The measured PSD for different landing energies of the electron beam. All other parameters are the same as in Figs. 4 and 5.

$$\mathrm{PSD}(f) = \frac{\Gamma(H + 1/2)}{\Gamma(H)} \frac{2\sqrt{\pi}\xi\sigma^2}{[1 + (2\pi f \xi)^2]^{H+1/2}}. \tag{7}$$

The 2-D-PSD can also be found from the autocovariance function of Eq. (5). To allow for different correlation lengths in the x and y directions, we replace $|x/\xi|$ by $\sqrt{(x/\xi_x)^2 + (y/\xi_y)^2}$:

$$R(x, y) = \frac{2^{1-H}\sigma^2}{\Gamma(H)} \left[\left(\frac{x}{\xi_x}\right)^2 + \left(\frac{y}{\xi_y}\right)^2\right]^{H/2} K_H\left(\sqrt{\left(\frac{x}{\xi_x}\right)^2 + \left(\frac{y}{\xi_y}\right)^2}\right). \tag{8}$$

The 2-D-PSD, Eq. (1), can be obtained by 2-D Fourier transformation

$$\mathrm{PSD}(f_x, f_y) = \int_{-\infty}^{\infty} \mathrm{d}x\, \mathrm{d}y\, e^{-2\pi i(f_x x + f_y y)} R(x, y), \tag{9}$$

$$\mathrm{PSD}(f_x, f_y) = \frac{4\pi H \sigma^2 \xi_x \xi_y}{[1 + (2\pi f_x \xi_x)^2 + (2\pi f_y \xi_y)^2]^{H+1}}. \tag{10}$$

For $\xi_x = \xi_y$, this equation reduces to the original isotropic form in the work of Palasantzas.[18]

10 Appendix D: Energy Dependence

The simulations in this paper were all done for 300-eV electron beams. The projection model, which follows from purely geometric arguments, works very well for this low landing energy. Higher landing energies lead to a larger "interaction volume" in which the electrons scatter. The result is an effective blur of the SEM image.

This effect is demonstrated in Fig. 15. It shows that increasing the landing energy leads to a suppression of the measured power at high frequencies. This effect is already significant at 1-keV beam energy.

Acknowledgments

References

1. G. F. Lorusso et al., "Need for LWR metrology standardization: the IMEC roughness protocol," *J. Micro/Nanolithogr. MEMS MOEMS* **17**(4), 041009 (2018).
2. C. Mack, "Systematic errors in the measurement of power spectral density," *J. Micro/ Nanolithogr. MEMS MOEMS* **12**(3), 033016 (2013).
3. A. Hiraiwa and A. Nishida, "Statistical- and image-noise effects on experimental spectrum of line-edge and line-width roughness," *J. Micro/Nanolithogr. MEMS MOEMS* **9**(4), 041210 (2010).

4. D. Goldfarb et al., "Effect of thin-film imaging on line edge roughness transfer to underlayers during etch processes," *J. Vac. Sci. Technol. B* **22**(2), 647–653 (2004).

5. J. Foucher, A. Fabre, and P. Gautier, "CD-AFM versus CD-SEM for resist LER and LWR measurements," *Proc. SPIE* **6152**, 61520V (2006).

6. G. Dahlen et al., "TEM validation of CD AFM image reconstruction: part II," *Proc. SPIE* **6922**, 69220K (2008).

7. R. Kizu et al., "Accurate vertical sidewall measurement by a metrological tilting-AFM for reference metrology of line edge roughness," *Proc. SPIE* **10959**, 109592B (2019).

8. S. George et al., "Characterization of line-edge roughness (LER) propagation from resists: underlayer interfaces in ultrathin resist films," *Proc. SPIE* **7636**, 763605 (2010).

9. V. Constantoudis et al., "Effects of resist sidewall morphology on line-edge roughness reduction and transfer during etching: is the resist sidewall after development isotropic or anisotropic?" *J. Micro/Nanolithogr. MEMS MOEMS* **9**(4), 041209 (2010).

10. J. Foucher et al., "Impact of acid diffusion length on resist LER and LWR measured by CD-AFM and CD-SEM," *Proc. SPIE* **6518**, 65181Q (2007).

11. M. Fouchier, E. Pargon, and B. Bardet, "An atomic force microscopy-based method for line edge roughness measurement," *J. Appl. Phys.* **113**(10), 104903 (2013).

12. M. Fouchier, E. Pargon, and B. Bardet, "A new method based on AFM for the study of photoresist sidewall smoothening and LER transfer during gate patterning," *Proc. SPIE* **8685**, 86850B (2013).

13. R. Lawson and C. Henderson, "Understanding the relationship between true and measured resist feature critical dimension and line edge roughness using a detailed scanning electron microscopy simulator," *J. Vac. Sci. Technol. B* **28**(6), C6H34–C6H39 (2010).

14. R. Lawson and C. Henderson, "Investigating SEM metrology effects using a detailed SEM simulation and stochastic resist model," *Proc. SPIE* **9424**, 94240K (2015).

15. T. Verduin et al., "The effect of sidewall roughness on line edge roughness in top-down scanning electron microscopy images," *Proc. SPIE* **9424**, 942405 (2015).

16. E. Thorsos, "The validity of the Kirchhoff approximation for rough surface scattering using a Gaussian roughness spectrum," *J. Acoust. Soc. Am.* **83**(1), 78–92 (1988).

17. C. Mack, "Generating random rough edges, surfaces, and volumes," *Appl. Opt.* **52**(7), 1472–1480 (2013).

18. G. Palasantzas, "Roughness spectrum and surface width of self-affine fractal surfaces via the K-correlation model," *Phys. Rev. B* **48**(19), 14472 (1993).

19. F. Salvat, A. Jablonski, and C. Powell, "ELSEPA—dirac partial-wave calculation of elastic scattering of electrons and positrons by atoms, positive ions and molecules," *Comput. Phys. Commun.* **165**(2), 157–190 (2005).

20. E. Schreiber and H.-J. Fitting, "Monte Carlo simulation of secondary electron emission from the insulator SiO_2," *J. Electron. Spectrosc. Relat. Phenom.* **124**(1), 25–37 (2002).

21. E. Palik, *Handbook of Optical Constants of Solids*, Five-Volume Set, Elsevier, Amsterdam, Netherlands (1997).

22. D. Penn, "Electron mean-free-path calculations using a model dielectric function," *Phys. Rev. B* **35**(2), 482–486 (1987).

23. H. Shinotsuka et al., "Calculations of electron stopping powers for 41 elemental solids over the 50 eV to 30 keV range with the full Penn algorithm," *Nucl. Instrum. Methods Phys. Res. Sect. B* **270**(1), 75–92 (2012).

24. T. Verduin, S. Lokhorst, and C. Hagen, "GPU accelerated Monte-Carlo simulation of SEM images for metrology," *Proc. SPIE* **9778**, 97780D (2016).

25. T. Verduin, P. Kruit, and C. Hagen, "Determination of line edge roughness in low-dose top-down scanning electron microscopy images," *J. Micro/Nanolithogr. MEMS MOEMS* **13**(3), 033009 (2014).

26. C. Mack and B. Bunday, "Using the analytical linescan model for SEM metrology," *Proc. SPIE* **10145**, 101451R (2017).

27. J. Villarrubia and B. Bunday, "Unbiased estimation of linewidth roughness," *Proc. SPIE* **5752**, 480–488 (2005).

28. E. Putna et al., "EUV lithography for 30-nm half pitch and beyond: exploring resolution, sensitivity, and LWR tradeoffs," *Proc. SPIE* **7273**, 72731L (2009).

29. L. van Look et al., "Optimization and stability of CD variability in pitch 40 nm contact holes on NXE:3300," *Proc. SPIE* **10809**, 108090M (2018).

30. S. Sinha et al., "X-ray and neutron scattering from rough surfaces," *Phys. Rev. B* **38**(4), 2297–2311 (1988).

Luc van Kessel received his master's degree in physics from Radboud University Nijmegen in 2017. Currently, he is a PhD student at Delft University of Technology. He works on the simulation of electron-matter interaction, with a particular focus on lithography applications.

Thomas Huisman received his master's degree in 2012 of the University of Twente, and his PhD in 2016 of the Radboud University, Netherlands. In 2017, he joined ASML as a researcher.

Cornelis W. Hagen received his master's degree in 1983 and his PhD in 1991 of the Free University of Amsterdam, Netherlands. He was a researcher at the Paul Scherrer Institute in Switzerland from 1989–1992, and at the Kamerlingh Onnes Laboratory of Leiden University, Netherlands, from 1992–1994. In 1994 he joined Delft University of Technology as an assistant professor and was appointed as associate professor in 2008. His area of research is microscopy and lithography with charged particles.